Textural and morphological studies on zinc–iron alloy electrodeposits

M KANAGASABAPATHY[a,*] and SOBHA JAYAKRISHNAN[b]

[a]Department of Chemistry, Rajapalayam Rajus' College, Affiliated to Madurai Kamaraj University, Rajapalayam 626 117, India
[b]EMFT Division, Central Electrochemical Research Institute, (Council of Scientific and Industrial Research), Karaikudi 630 003, India
e-mail: rjpmks@yahoo.com

Abstract. Zinc–iron alloy electrodeposits have industrial significance, since they provide better corrosion resistance and with improved mechanical properties when compared to pure zinc coatings. This is due to the unique phase structure of the alloy formed. But this deposition belongs to anomalous deposition, where the electrochemically less noble zinc deposits more preferentially, than the more noble iron. So the industrial process control over the deposition becomes difficult. So, this study correlates the effect of various deposition parameters over the deposition kinetics and deposited alloy characteristics. Transition and partial current densities were computed. Effect of hydrogen overpotential and surface coverage due to the adsorbed intermediates over anomalous deposition were explored. Plausible deposition mechanism and mathematical model was proposed to predict the anomalous electrodeposition characteristics. Textural, morphological and phase structural characteristics of the alloy was investigated. By the substitution of iron in the hcp lattice, c/a ratio was lowered and the lattice geometry was distorted. Intermetallic compounds of variable composition such as $FeZn_{14}$, Fe_5Zn_{33}, Fe_3Zn_{13} and $FeZn_3$ with 'η' and 'Γ' phase structures were noted. Electrodeposition parameters were optimized and smooth, adherent, strain-free deposits with required iron content and hardness were obtained.

Keywords. Zinc–iron alloy; anomalous electrodeposition; texture; morphology.

1. Introduction

Zinc coating is the most promising technique, to protect steel components from corrosion, since zinc is anodic to iron ($E^0_{Zn} = -0.76$ V and $E^0_{Fe} = -0.44$ V) and it provides sacrificial protection to steel. But under severe corrosive environments, zinc coating depletes rapidly from the steel surface. So to enhance the degree of protection and to meet the modern industrial standards, different zinc alloy coatings were studied. Among the various zinc alloy coatings, zinc alloyed with iron group metals[1–6] (Fe, Ni, Co) are having industrial significance since these alloy coatings are cathodic to pure zinc coatings but anodic to steel components. This study investigates specifically, the characteristics of zinc–iron alloy electrodeposition, since this zinc–iron alloy deposits provide three times higher corrosion resistance when compared to pure zinc deposits. In addition to that, due to the unique phase structure of the zinc–iron alloy, this coating has better mechanical properties[7,8] such as hardness, adherence, weldability, etc. In order to get the desired degree of protection and mechanical properties, the coating should contain about 15–25 weight percent of iron.[9–11] But unlike other alloy deposition, this zinc–iron group alloy deposition belongs to anomalous co-deposition,[12–14] where the electrochemically less noble zinc deposits more preferentially than the more noble iron group metals. So the industrial process control over the zinc–iron deposition becomes difficult. This study investigates the effect of various deposition parameters over the electrodeposition characteristics and the micro structural nature of the zinc–iron alloy formed.

2. Experimental

Electrodeposition of zinc–iron alloy was carried out from the sulphate bath. The optimized composition of the bath used for this study is as follows: $[ZnSO_4 \cdot 7H_2O]$ – 0.28 M; $[FeSO_4 (NH_4)_2 SO_4 6H_2O]$ – 0.41 M and [KCl] – 1.07 M. In the bath, KCl was added to enhance the specific conductance[15] and

secondary current distribution. A small amount of disodium salt of EDTA (0.08 M) was added to improve the bath stability.[16] Deposition was done over mechanically polished and electrocleaned mild steel panels of size 5.0 cm × 2.5 cm × 0.05 cm, under galvanostatic conditions by means of three electrode assembly, using a DC regulated power supply, (Aplab L3230 model, India make). The anode used was electrolytic grade zinc, with the same dimensions to that of cathode. Cathodic overpotential (η_c) was measured at every 30 seconds at a given cathodic current density (i_c) with reference to saturated calomel electrode through a Luggin probe assembly.[17] Composition of this alloy was analysed by Energy Dispersive X-ray Analyser (Hitachi S–3000H model). Deposition was also carried out simultaneously, over mechanically polished and electrocleaned stainless steel panels of size 5.0 cm × 2.5 cm × 0.05 cm, under the given conditions. After weighing, the alloy was dissolved in 20 volume percent nitric acid and this solution was made up to 100 ml. The alloy composition was then analysed by using Atomic absorption spectrophotometer (VARIAN Model SPECTRAA 220 model). Composition of the alloy was expressed in the weight percentage of iron (p_{Fe}).

Based on the three electrode assembly, potentiostatic studies over glassy carbon electrode was carried out, by using Autolab PGSTAT 30 electrochemical analyzer (The Netherlands make). Glassy carbon electrode of area 0.25 cm^2 (Tokai Carbon Company, Japan make) was used as the working electrode. Platinum foil of 2.5 cm × 2.5 cm area was used as the counter electrode and saturated calomel electrode was used as the reference electrode. To eliminate the interference of oxygen, bath was purged by passing pure nitrogen for one hour.

Adhesion of the deposit over substrate was tested by the standard qualitative bend test to an angle of 180° with a deposit thickness of 25×10^{-6} m. Microhardness of the coating was measured in Vicker's hardness number (VHN) by static indentation method, using Leco microhardness tester (Model M 400) at a given load for 15 seconds time duration. X-ray diffraction patterns were taken by using JEOL PANalytical, X' per PRO model. Samples were scanned between 20° and 80°, 2θ at a rate of 1° min^{-1} using Cu K$_\alpha$ (λ = 1.54 A°) radiation. The hkl values were interpreted in accordance with ICDD.[18] Lattice parameters such as 'c' and 'a' were computed based on d-spacing values for the given hkl planes. Scanning electron microscopic (SEM)

images were obtained by using Hitachi S–3000H model.

3. Results and discussion

3.1 *Electrochemical kinetics*

Effect of current density, temperature and stirring of the bath over the weight percentage of the iron in the alloy composition (p_{Fe}) was studied and given in figure 1. Iron content in the alloy increased, if the current density (i_c) was increased (table 1). Though the weight percentage of iron in the bath was higher than zinc, the deposit has lower iron percentage than that of bath CR (Composition Reference) Line. At the same time if the bath temperature was increased or if the bath was stirred then the iron content in the alloy lowered.
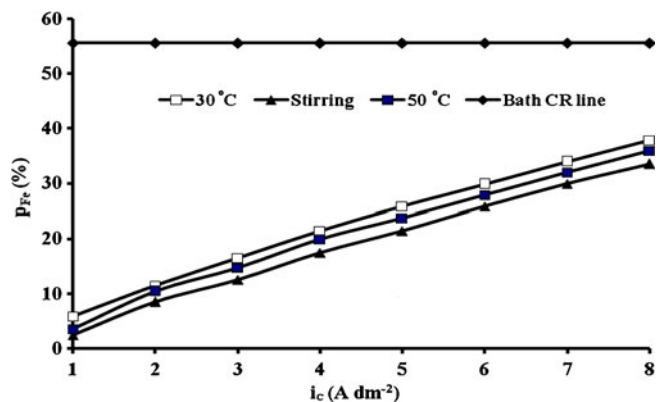

Figure 1. Effect of deposition parameters over alloy composition.

Table 1. EDAX data of alloy composition at different current densities and at 30°C.

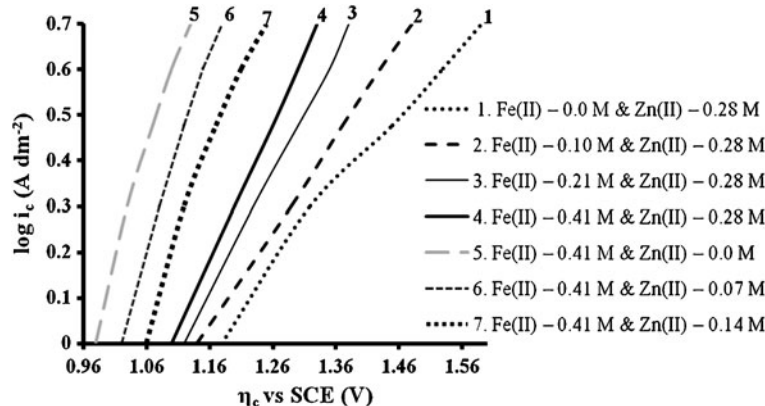| Sl No.	i_c (A dm^{-2})	Alloy composition (weight percent)	
		Zinc	Iron
1.	1	94.2	5.8
2.	2	88.6	11.4
3.	3	83.5	16.5
4.	4	78.6	21.4
5.	5	74.2	25.8
6.	6	70.2	29.8
7.	7	66.1	33.9
8.	8	62.2	37.8

Figure 2. Tafel plot for the variation of Fe^{2+} and Zn^{2+} concentrations.

Tafel plot for the variation of Fe^{2+} and Zn^{2+} concentration under galvanostatic condition was given in figure 2. This shows that if the concentration of Fe^{2+} in the bath was increased, then the cathodic overpotential shifted less negatively. The current density obtained by extrapolation of polarization data values[19] (i_o) were noted from figure 2. It decreased, if the Fe^{2+} concentration was increased. The value was about 1.99×10^{-4} A dm^{-2} at 0.41 M and about 1.58×10^{-2} A dm^{-2} in the absence of Fe^{2+}. Similarly, potentiostatic studies were carried out (figure 3) and from this it was observed that in presence of Fe^{2+} the cathodic current was increased but the cathodic peak potential was shifted less negatively in forward scan. So it was confirmed that in presence of Fe^{2+}, the overall cathodic potential was reduced, due to the lowering of deposition rate by

kinetic control processes. But the anodic peak potential was shifted less negatively and during the reverse scan two anodic peaks were noted. This shows that the alloy dissolution[20,21] takes place under two different potential values. Zinc-rich alloy undergoes anodic dissolution at more negative potential (-0.725 V) whereas iron-rich alloy undergoes dissolution at less negative anodic potential (-0.585 V).

From these studies it can be revealed that the deposition of iron is hindered by charge-transfer control process at lower i_c values, where as the deposition rate of zinc is lowered by mass-transport limitations at relatively higher i_c values. Though the interface is enriched with Fe^{2+}, at lower i_c values, its deposition rate is impeded due to charge-transfer limitations. But it was shown by Gomez *et al.*[22] at higher i_c values the deposition rate of Zn^{2+} is very high in the initial stages of deposition when compared to Fe^{2+}. And this leads to rapid depletion of Zn^{2+} at the electrode–electrolyte interface. But due to the mass transfer limitations of Zn^{2+} (from bulk to electrode interface), deposition rate of Fe^{2+} is enhanced. The mass transfer limitations of Zn^{2+} can be lowered by convection process such as through bath stirring or by increasing the bath temperature. By the forced convection, the diffusion layer is quickly enriched with Zn^{2+} and so the deposition rate of zinc can be increased.
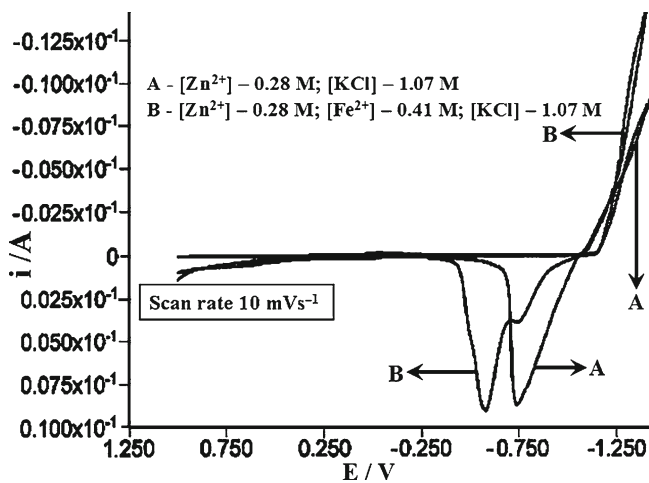
3.2 *Mathematical correlation*

The value of weight percentage of iron content of the alloy, $p_{Fe}(x)$ at a given cathodic current density, $i_c(x)$ was predicted using Lagrange interpolation of irregular intervals. Values of apparent current densities,

Figure 3. Potentiostatic studies.

$i_c(1)$, $i_c(2)$ ... $i_c(n)$ and its corresponding weight percentage of iron content of the alloy $p_{Fe}(1)$,
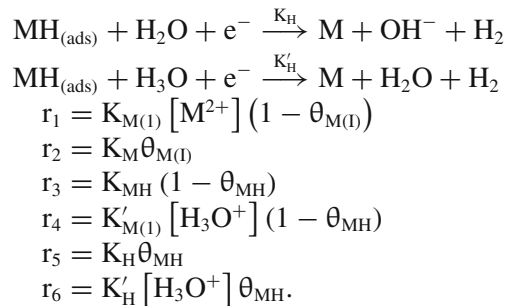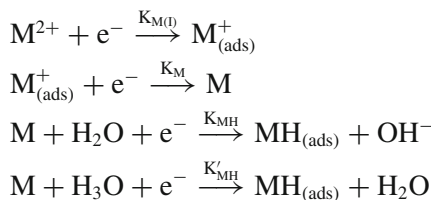
$p_{Fe}(2)$ ... $p_{Fe}(n)$ can be correlated by the following relation:

$$p_{Fe}(x) = \frac{\{[i_c(x) - i_c(2)] \times [i_c(x) - i_c(3)] \times \ldots \times [i_c(x) - i_c(n-1)] \times [i_c(x) - i_c(n)]\} \times p_{Fe}(1)}{\{[i_c(1) - i_c(2)] \times [i_c(1) - i_c(3)] \times \ldots \times [i_c(1) - i_c(n-1)] \times [i_c(1) - i_c(n)]\}}$$
$$+ \frac{\{[i_c(x) - i_c(1)] \times [i_c(x) - i_c(3)] \times \ldots \times [i_c(x) - i_c(n-1)] \times [i_c(x) - i_c(n)]\} \times p_{Fe}(2)}{\{[i_c(2) - i_c(1)] \times [i_c(2) - i_c(3)] \times \ldots \times [i_c(2) - i_c(n-1)] \times [(i_c(2) - i_c(n)]\}}$$
$$+ \ldots + \frac{\{[i_c(x) - i_c(1)] \times [(i_c(x) - i_c(2)] \times \ldots \times [(i_c(x) - i_c(n-2)] \times [(i_c(x) - i_c(n)]\} \times p_{Fe}(n-1)}{\{[i_c(n-1) - i_c(1)] \times [i_c(n-1) - i_c(2)] \times \ldots \times [i_c(n-1) - i_c(n-2)] \times [i_c(n-1) - i_c(n)]\}}$$
$$+ \frac{\{[i_c(x) - i_c(1)] \times [i_c(x) - i_c(2)] \times [i_c(x) - i_c(3)] \times \ldots \times [i_c(x) - i_c(n-1)]\} \times p_{Fe}(n)}{\{[i_c(n) - i_c(1)] \times [i_c(n) - i_c(2)] \times [i_c(n) - i_c(3)] \times \ldots \times [i_c(n) - i_c(n-1)]\}}.$$

Based on this the weight percentage of iron content in the alloy, p_{Fe} at a given i_c value at 30°C can be correlated by the following II order polynomial equation: $p_{Fe} = -ai_c^2 + bi_c$, where $a \approx 0.15$ and $b \approx 4a$. The experimentally determined alloy composition at a given i_c, was concurred with predicted values and less than $\pm 2.0\%$ deviation was observed over the range of i_c values studied. The transition current density, i_t (at which anomalous deposition becomes normal co-deposition) at 30°C was determined under galvanostatic condition and it was 14.2 Adm^{-2}. The corresponding weight percent of iron in the alloy is 56.28. The deviation from the predicted value was found to be -1.2231%.

3.3 *Effect of hydrogen overpotential*

Partial current density values were determined and correlated to the surface coverage of metal intermediates formed, under the influence of hydrogen evolution reaction (HER). Based on the Volmer, Tafel and Heyrovsky models of HER and subsequent surface coverage of intermediates adsorbed, following mechanisms were proposed. M^+ and M^{2+} represents metal ions or mono hydroxides[23–27] or di hydroxides and $\theta_{M(I)}$, and θ_{MH} are cathodic surface coverage of M^+ (metal ions or their corresponding hydroxides) and MH (metal hydrides) respectively through adsorption. r_1, r_2 ... r_6 are rate of the relevant reactions.

$$M^{2+} + e^- \xrightarrow{K_{M(I)}} M^+_{(ads)}$$
$$M^+_{(ads)} + e^- \xrightarrow{K_M} M$$
$$M + H_2O + e^- \xrightarrow{K_{MH}} MH_{(ads)} + OH^-$$
$$M + H_3O + e^- \xrightarrow{K'_{MH}} MH_{(ads)} + H_2O$$

$$MH_{(ads)} + H_2O + e^- \xrightarrow{K_H} M + OH^- + H_2$$
$$MH_{(ads)} + H_3O + e^- \xrightarrow{K'_H} M + H_2O + H_2$$
$$r_1 = K_{M(I)} [M^{2+}] (1 - \theta_{M(I)})$$
$$r_2 = K_M \theta_{M(I)}$$
$$r_3 = K_{MH} (1 - \theta_{MH})$$
$$r_4 = K'_{M(I)} [H_3O^+] (1 - \theta_{MH})$$
$$r_5 = K_H \theta_{MH}$$
$$r_6 = K'_H [H_3O^+] \theta_{MH}.$$

Based on this the effective partial current density values for iron (i_{Fe}) as well as zinc (i_{Zn}) deposition and for hydrogen evolution (i_H) were determined and given in figure 4. The value of i_{Fe} was always lower than i_H value, at all current densities studied. This shows that the overall decomposition rate of the iron intermediates is lower than the decomposition rate of zinc intermediates. The estimated[28] value of hydrogen overpotential for iron is about 0.53 V and for zinc 0.75 V at a concentration of $[H^+] = 1$ M at 1 Adm^{-2}. So it can be noted that the HER competes with the iron deposition rate rather than with zinc deposition rate. From this it can be
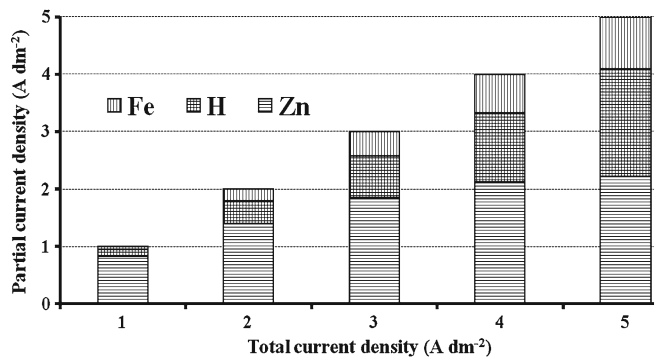

Figure 4. Effective partial current density values.

elucidated that, though the interface was enriched with the Fe^{2+}, reduction rate of iron was hindered by charge transfer limitations.

3.4 *XRD studies*

XRD patterns of the deposits at different current densities are given in figure 5. Pyramidal textural intensity was significant than the prismatic and basal textures. Generally, (101)hcp peak was present almost in all deposits with significant intensity. The peak noted at the 2θ value of 77° was indexed to (004) plane. Textural intensity was relatively higher for the deposits obtained 2 A dm^{-2}. (200)α peak for iron was noted distinctly above 2 A dm^{-2}. Certain peaks representing specific crystallographic hkl plane gradually shifted either to higher or lower 2θ angles with the change in iron content in the deposit. Both 002 and 102 peak shifted to higher 2θ, whereas 100 peak shifted to lower 2θ, when the iron content in the deposit was increased. The 101 peak was not shifted significantly. These observed results are in accordance with previous reports. [29,30] Interplanar spacing (d) for different hkl planes and the axial ratio (c/a) for deposits obtained at different i_c values are given in figure 6. Axial ratio value decreased from 1.86 (at 1 Adm^{-2}) to 1.66 (at 5 Adm^{-2}) or if the iron content was increased as observed by Kondo[31,32] *et al.* This is due to lowering of the value of 'c' and the value of 'a' is almost constant for the hkl planes studied. This showed that the
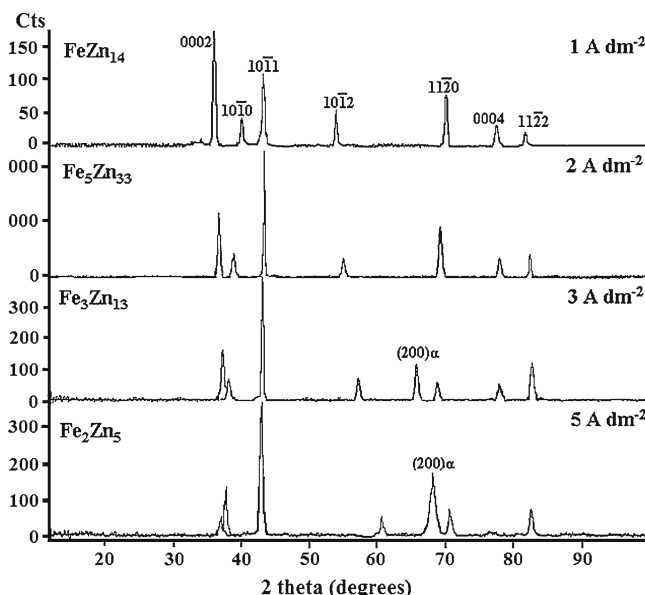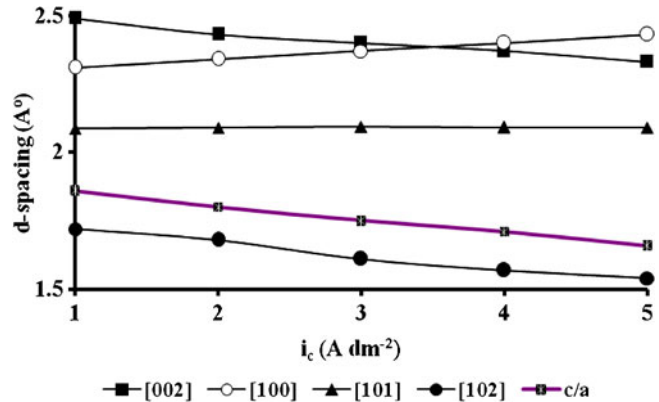

Figure 6. d–spacing and c/a values of deposits for different i_c values.

hcp lattice geometry distorted, if the iron content was increased and the probability of substitution of iron along c-axis is more than a-axis, because the linear density along c-axis is lower. In other words the basal plane is tightly packed (six atoms) than the axial plane (three atoms).

Peak broadening due to internal lattice strain[33] was not notified from the observed full width at half maxima (FWHM) values. This shows that adherent and strain free deposits were obtained under the conditions studied. The deposited alloy belongs to intermediate phase type, since the crystal structures of both metals are not same and the atomic volume ratio of iron to zinc is, ∼80%. So, the substitution of iron atom in the hcp lattice, leads to change the lattice geometry and it lowers the axial ratio.

3.5 *Morphological characteristics*

From SEM images [figure 7], it was observed that the deposit morphology[34] was influenced by the alloy composition. Three types of morphologies were observed. For zinc-rich alloy (<10% iron content), distorted hexagonal (1 A dm^{-2}) morphology was noted. For an alloy with optimum (10–25%) iron content, triangular pyramidal morphology (2–4 A dm^{-2}) was observed. Relatively smooth and compact deposit with fine-grained morphology (with an iron weight percentage of ≈ 17%) was noted at 3A dm^{-2}. Coarser deposits with stacked platelet coloumnar morphology were noted above 5 A dm^{-2} (iron content >25%).

Reduction of crystallite size at 3 A dm^{-2} indicates that the nucleation rate was higher than the grain growth rate. This indicates the overall deposition rate was predominantly controlled by charge-transfer processes rather than mass-transfer processes. But at higher
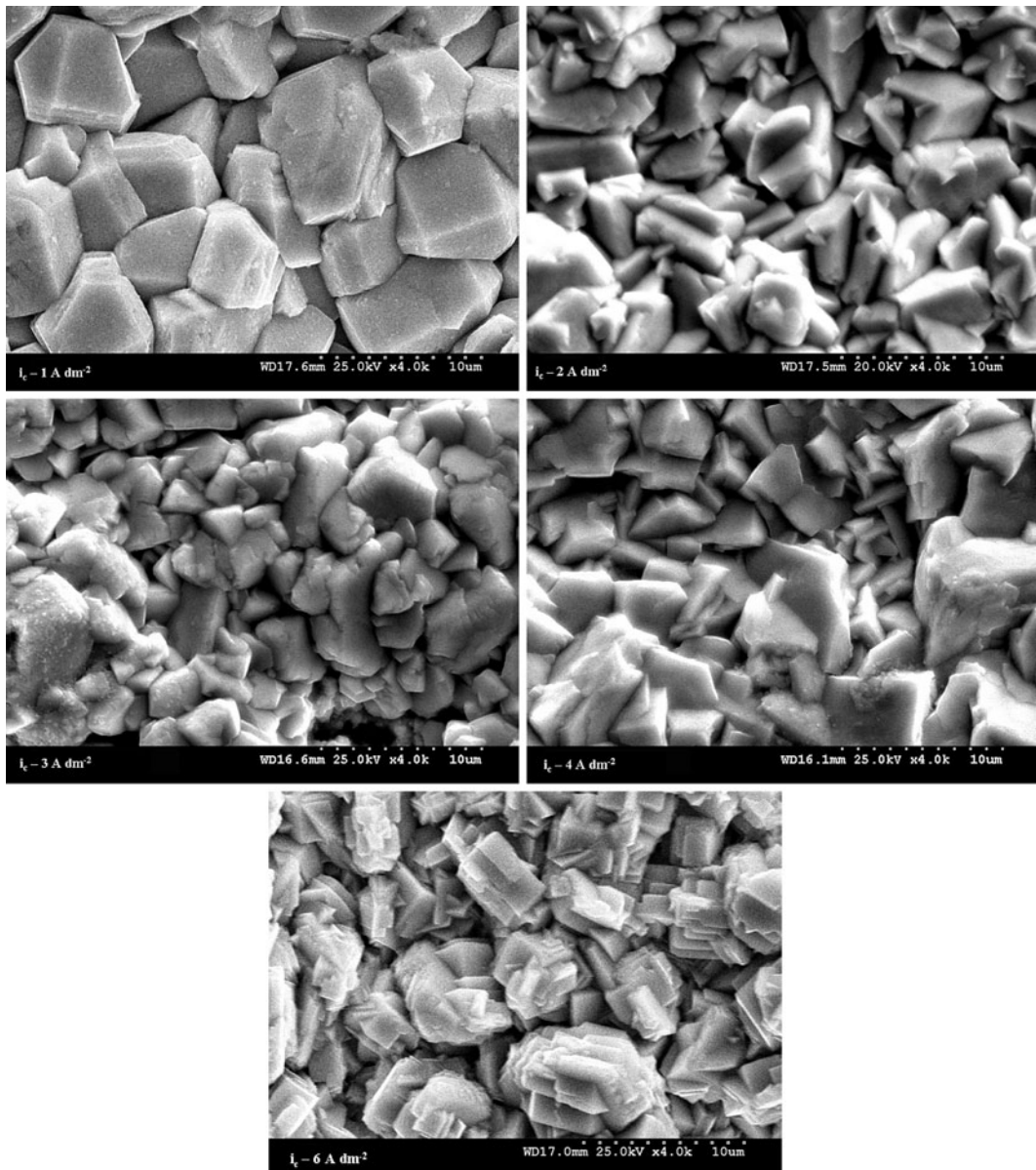

Figure 5. XRD patterns of the deposits for different i_c values.

Figure 7. SEM images of deposits for different i_c values.

current densities (above 5 A dm^{-2}) the overall deposition rate was controlled by mass transfer limitations particularly for zinc. So the grain growth rate was higher than the nucleation rate and this leads to the formation of coarser morphology enriched with iron.

3.6 *Microhardness*

Through the repeated standard qualitative bend test[35] it was observed that the deposits were highly adherent to the substrate without internal strain. Microhardness of the deposits obtained at 1 Adm^{-2} was found to be 120.6 VHN and it increased to 156.7 VHN at 5 Adm^{-2}. Microhardness of the deposit increased, if the iron

content in the alloy was increased, since the hardness of the iron is relatively higher than the zinc. This microhardness value reflects the resistance of this coating towards plastic deformation and the abrasion resistance of this zinc–iron alloy coating is higher than pure zinc coating.[36,37]

3.7 *Phase structure*

Very few studies with contrary views,[31,32,38] over this alloy phase structure were reported. The phase structure of this electrodeposited alloy is different from thermally formed alloy phase structure. At lower iron content, (<10% Fe) 'η' phase was dominant and if the

iron content of the alloy was increased ($>10\%$ Fe) then the 'Γ' phase augmented. Formation of phase structures can be correlated based on the composition of the alloy formed and deposition kinetics of metal ions. At lower current densities, the mass transport limitations for Zn^{2+} are not significant when compared to charge-transfer restrictions of Fe^{2+}. So its grain growth rate is higher than that of nucleation rate. Hence the deposition of zinc ad-atoms are taking place gradually, leads to the formation of zinc-rich, distorted hcp 'η' phase. However, at higher current densities, the overall deposition process is limited by diffusion control processes. Due to this, the deposition rate of Zn^{2+} at the electrode interface is very fast when compared to its diffusion rate from the bulk of the solution. So, the electrode interface is enriched with Fe^{2+} due to the quick depletion of Zn^{2+} and this reduces the kinetic control limitations of Fe^{2+}. So the 'Γ' phase is formed, by the adsorption of iron ad-atoms over the surface of previously formed zinc-rich 'η' phase.

Based on Hume–Rothery's rule this alloy belongs to intermetallic compounds of variable composition with metastable structures and exist as electron compounds of D-8_2 structure.[31] It was observed that the low iron content intermetallic compounds such as $FeZn_{14}$, have dominantly 'η' phase structure whereas the intermetallic compounds with moderate iron content, like Fe_5Zn_{33}, Fe_3Zn_{13} and $FeZn_3$ are exist as with 'Γ' phase structure.

4. Conclusion

Anomalous electrodeposition behaviour of iron in the zinc–iron alloy formation was studied based on sulphate bath under galvanostatic and potentiostatic conditions. From the deposition kinetics and from the i_o values, it was observed that, the overall deposition rate of iron was significantly reduced by charge-transfer process though the interface was enriched with Fe^{2+}. The deposition rate of zinc was lowered only if the deposition was under diffusion controlled conditions. Under the mass transfer limitations of Zn^{2+}, deposition rate of iron at the electrode interface was enhanced. From the hydrogen overpotential and transition as well as partial current density measurements, it was noted that the surface adsorbed intermediates appreciably favoured for HER rather than the reduction of Fe^{2+}. The observed alloy content under the given cathodic current densities concurred with the proposed mathematical model. (101)hcp plane was present almost in all deposits with significant intensity. If the iron content in the alloy was increased, c/a ratio decreased and also the hcp lattice geometry distorted, due to the substitution of iron along c-axis rather than a-axis. Distorted hexagonal morphology of the alloy was changed to triangular pyramidal and then to coloumnar structure, if the cathodic current density was increased. Microstructures of the alloy formed can be interpreted from the deposition rate. It was noted that the low iron content compounds such as $FeZn_{14}$, have 'η' phase structure and the moderate iron content compounds, like Fe_5Zn_{33}, Fe_3Zn_{13}, $FeZn_3$ have 'Γ' phase structure. The alloy composition and microstructure can be controlled through the proposed models. Smooth, adherent, strain-free deposits with required iron percentage and hardness were obtained as per industrial standards.

References

1. Lin Y P and Selman J R 1993 *J. Electrochem. Soc.* **140** 303
2. Baldwin K R and Smith C J E 1996 *Trans. IMF.* **74**, 202
3. Crotty D 1996 *Met. Fin.* **9** 54
4. Zaki N 1999 *Prod. Fin.* **63** 53
5. Pushpavanam M 2000 *Bull. Electrochem.* **16** 559
6. Abou Krisha M M, Assaf F H and Toghan A A 2007 *J. Solid State Electrochem.* **11** 244
7. Pech Canul M A, Ramanauskas R and Maldonado L 1997 *Electrochim. Acta* **42** 255
8. Hixon H G and Sherwood P M A 2001 *J. Phys. Chem.* **105** B 3957
9. Herb Geduld 1988 *Zinc Plating* (Ohio: ASM International, vol. 11, p. 237)
10. Sylla D, Savall C, Gadouleau M, Rebere C, Creus J and Refait Ph 2005 *Surf. Coat. Technol.* **200** 2137
11. Narasimhamurthy V and Sheshadri B S 1997 *Met. Fin.* **9** 44
12. Dahms H and Croll I M 1965 *J. Electrochem. Soc.* **112** 771
13. Higashi K, Fukushima H, Urakawa T, Takeshi Adaniya and Kazuo Matsudo 1981 *J. Electrochem. Soc.* **128** 2081
14. Tsuru T, Kobayashi S, Akiyama T, Fukushima H, Gogia S K and Kammel R 1997 *J. Appl. Electrochem.* **27** 209
15. An M, Zhang J, Yang Z and Wang H 1996 *Mater. Prot. (China)* **29** 12
16. Naik Y A, Venkatesha T V and Nayak P V 2002 *Turk. J. Chem.* **26** 725
17. Eliezer Giledi 1993 *Electrode kinetics* (New York: VCH Publishers Inc, vol. 8, p. 45)
18. International Centre for Diffraction Data, PDF-2, (JCPDS) 2000, Database 1- 49, Pennsylvania
19. Fratesi R and Roventi G 1989 *Mater. Chem. Phys.* **23** 529
20. Pickering H W and Wagner C 1967 *J. Electrochem. Soc.* **114** 698

21. Ravindran V and Muralidharan V S 2007 *Trans. IMF.* **85** 153
22. Gomez E, Pelaez E and Valles E 1999 *J. Electroanal. Chem.* **469** 139
23. Grande W C and Talbot J B 1993 *J. Electrochem. Soc.* **140** 675
24. Matlosz 1993 *J. Electrochem. Soc.* **140** 2272
25. Vaes J, Franser J and Celis J P 2000 *J. Electrochem. Soc.* **147** 3718
26. Diaz S L, Mattos O R, Barcia O E and Fabri Miranda F J 2002 *Electrochim. Acta.* **47** 4091
27. Elumalai P, Vasan H N, Munichandraiah N and Shivashankar S A 2002 *J. Appl. Electrochem.* **32** 1005
28. *Handbook of Electrochemistry*, 2008, Society for Advancement of Electrochemical Science and Technology (SAEST), Karaikudi, Tamilnadu, India, 1.3, 4
29. Park H and Szpunar J A 1998 *Corro. Sci.* **40** 525
30. Karahan I H 2007 *J. Mater. Sci.* **42** 10160
31. Kondo K, Hinotani S and Ohmori Y 1988 *J. Appl. Electrochem.* **18** 154
32. Czerwinski F, Kondo K and Szpunar J A 1997 *J. Electrochem. Soc.* **144** 481
33. Drewien C A, Goldstein J I and Marder A R 1994 *Metall. Mater. Trans.* **25** A 249
34. Kondo K, Yokoyama M and Shinohara K 1995 *J. Electrochem. Soc.* **142** 2256
35. Dini J W 1992 *Electrodeposition—The materials science of coatings and substrates* (New York: Noyes Publications, vol. 3, p. 56)
36. Narasimhamurthy V and Sheshadri B S 1996 *J. Appl. Electrochem.* **26** 90
37. Panagopoulos C N, Agathocleous P E, Papachristos V D and Michaelides A 2000 *Surf. Coat. Technol.* **123** 62
38. Czerwinski F, Kondo K and Szpunar J A 1998 *J. Mater. Sci.* **33** 2589